

Nanopore and tunneling resonance in an open kink in carbon nanotubes

Alex Kleiner

orcid.org/0000-0002-4694-2218

(Dated: March 10, 2023)

In weakly buckled carbon nanotubes, the kink is an open, ovalized constriction – where molecular-sized analytes and ions can pass. Moreover, in semiconducting tubes, the kink has an electronic bound state within the bandgap. This state is localized, hence highly susceptible to electrostatic perturbation by a proximate, itinerant ion. The degree to which this perturbation will modulate the electronic current – which is our signal, can be maximized in a tunnel-junction set-up, near resonance. We thus propose such a device, analyse its performance and, since the bound state depends on the post-buckling bending, suggest a scalable fabrication method to achieve bending and buckling of carbon nanotubes to an adjustable degree.

1. Introduction

Solid-state nanopore devices may revolutionize medicine [1] but have poor signal-to-noise ratios compared with biological ones [2]; their pores, fabricated by top-down methods, are inherently larger and rougher. In addition, all label-free nanopore devices work by ionic-current blockade, which is hard to scale.

Here we propose a scalable solid-state nanopore device with a smooth and adjustable "pore" where the signal is electronic. The proposed pore is a shallow, ovalized kink (hereafter: open kink), in a buckled semiconducting carbon nanotube (CNT). The highly localized kink deformation affects both ionic and electronic currents: depending on the tube type and degree of curvature, it may form a potential well or barrier [3] for conduction electrons. Hence, a passing ion, by effectively gating the surrounding local potential, can modify the electronic current, especially when the current is due to tunneling. This concept can be applied, in principle, to all semiconducting tubes (barring in mind the differences [3]), but throughout this work, the derived results are quantitatively exemplified with a specific tube: the zigzag (10,0).

First, however, we describe the proposed method of bending and buckling the tube so that its final bending curvature (and thus, the depth of the kink's localized bound state) could be determined in the initial lithographic patterning stage.

2. Layout of the device

In the following we discuss the physical realization of the kink junction (fig. 1, see also [4]). Consider a tube deposited on a pre-patterned trench or step as in fig. (1a). In it, there are two metal types: metal I, which is a "normal" metal with high melting point, and metal II with a low melting point (but above room temperature), such as Gallium. The tube is then clamped to the column in the trench with a normal metal electrode (metal I) and additional layer of oxide (together, forming the so-called structural layer). The entire layout in fig. (1a) is assumed to be grown at a lower temperature than the

melting point of metal II.

Upon raising the temperature above the melting point of metal II, the droplet adopts a new conformation (fig. 1b) with the wetting angle ϕ given by,

$$\gamma_{II} \cos \phi + \gamma_{I-II} = \gamma_o, \quad (1)$$

where γ_{II} , γ_{I-II} , γ_o are the surface tensions of metal II, interface of metals I and II and oxide, respectively.

Assuming the in-plane dimension of the layout is $\gg d$ and large enough so that resistance from the bending tube does not notably affect the final conformation, then by elementary geometry we get,

$$\Delta h = h + \frac{1}{2} \left(f(\phi)d - \sqrt{4hf(\phi)d + f(\phi)^2 d^2} \right), \quad (2)$$

where

$$f(\phi) = \frac{4 \sin^2 \phi}{2\phi - \pi - \sin 2\phi}.$$

Fig. (2) depicts the height change for a number of aspect ratios according to eq. (2).

The bent section (fig. 1b), at the onset of buckling, has a curvature of

$$\kappa = \frac{2\Delta h}{(\Delta h)^2 + \Delta^2}. \quad (3)$$

The critical curvature at which CNTs buckle was found by MD simulations to depend on the tube radius in accordance with continuous elasticity theory,

$$\kappa^{\text{cr}} = \frac{A}{R^2} \quad (4)$$

where the value of A found by different groups somewhat varies ($A = 0.385\text{\AA}$ by [5], 0.376\AA by [6] and 0.185\AA according to [7]; see also [8]). Thus, in order to induce buckling, ($\kappa \geq \kappa^{\text{cr}}$), the height of the structural layer h (fig. 1b) must be lowered by,

$$\Delta h \geq \frac{R^2}{A} - \sqrt{\frac{R^4}{A^2} - \Delta^2}, \quad (5)$$

where $\Delta \leq R^2/A$. To see what h and Δ might be, consider tubes in the range (10,0) to (20,0), having $R = 4\text{\AA}$

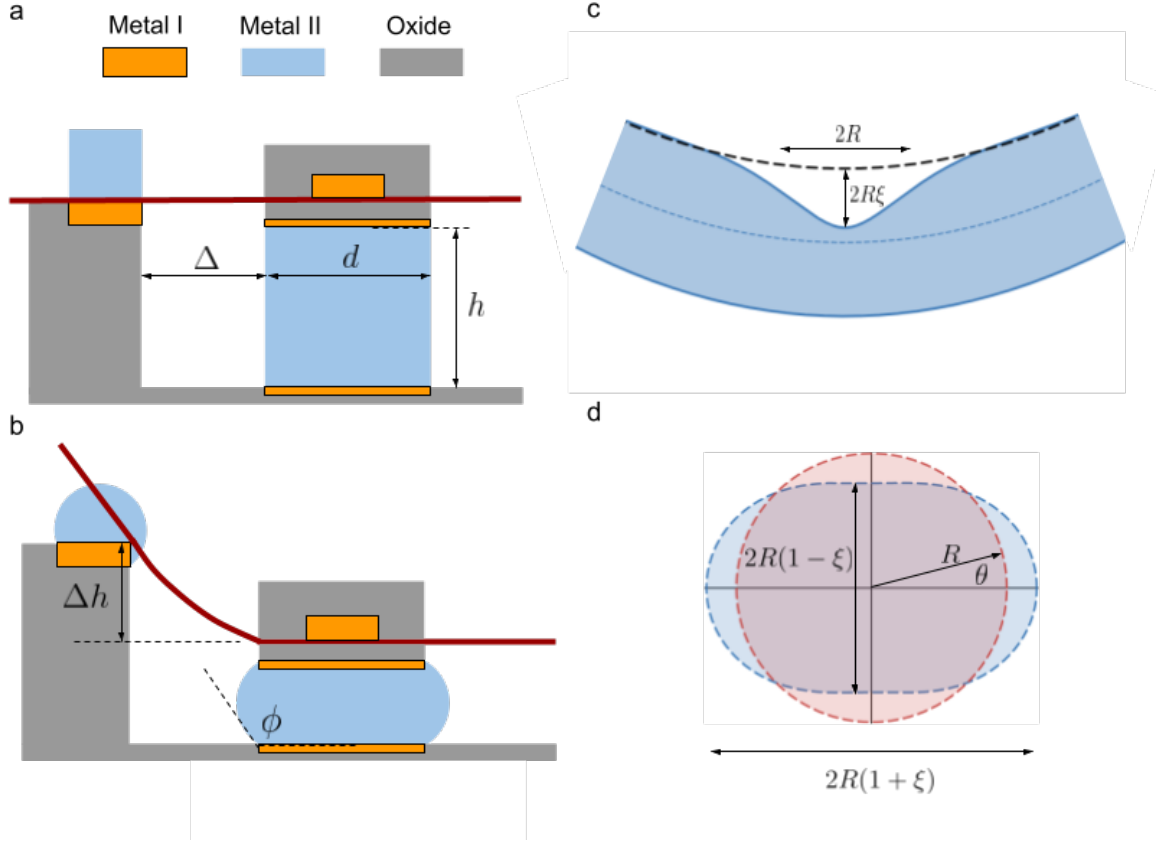


Figure 1: (a)-(b) Main two steps. Metal II has a low melting-point T_m , but the structure was deposited at $T < T_m$. On raising the temperature $T > T_m$, metal II melts and wets metal I (which remains solid and fixed to the oxide substrate). Capillary forces pull down the structural layer including the tube. (c) Open kink profile. The kink's width $W \sim 2R$. (d) Kink's cross-section as parametrized by the ovalization parameter ξ , having $R \rightarrow R(1 + \xi \cos 2\theta)$. At the onset of buckling its already slightly ovalized at $\xi = 2/9$ (blue shape). The closing of the kink corresponds to ξ^{close} (eq. 8).

and 8\AA , respectively. Taking $A = 0.185\text{\AA}$ [7], eq. (5) gives $h = \Delta$, where $\Delta \leq 8.65\text{nm}$ for the (10,0) tube, and $\Delta \leq 34.6\text{nm}$, for the (20,0) one. These are rather small values but we need to keep in mind that local imperfections are likely to reduce the critical curvature, hence the values given for A here should be treated as an ideal upper limit.

3. Open kink

The elasticity of carbon nanotubes was found, both experimentally [9][10] and by simulations [9][5][8][7][6][11], to conform to the elasticity of thin cylindrical shells within continuous elastic theory [12]. Their properties under bending and buckling were explained by Brazier a century ago [13]. In a previous work we summarize this theory as applied to single-walled CNTs ([3] - appendix A).

MD-simulations of bent CNTs [14] uncovered two crit-

ical points: the buckling curvature κ^{cr} which marks the onset of the kink, and a second curvature κ^{close} , which marks the closing of the kink's cross-section. The region between them is called the *transient regime* [14]. It is characterized by having an open kink with an ovalized, bending-dependent, cross-section. This work requires an open kink and thus lies entirely within the transient regime.

The ovalization parameter of the open kink, ξ^{kink} , is given by [3],

$$\xi^{\text{kink}} = \frac{2}{9} + \left(\xi^{\text{close}} - \frac{2}{9} \right) \tilde{\kappa}^{1/2}, \quad (6)$$

where

$$\tilde{\kappa} \equiv \frac{\kappa - \kappa^{\text{cr}}}{\kappa^{\text{close}} - \kappa^{\text{cr}}}, \quad \text{having } \kappa^{\text{cr}} \leq \kappa \leq \kappa^{\text{close}}, \quad (7)$$

and κ^{close} is the bending curvature at which the kink

closes: i.e: its ovalization parameter,

$$\xi^{\text{close}} \equiv 1 - \frac{d_g}{2R}, \quad (8)$$

corresponds to maximum flattening of the cross-section: i.e: where the distance between the opposite walls of the kink equals the inter-layer distance in graphite ($d_g = 3.35\text{\AA}$). A (10,0) tube, with $R = 4\text{\AA}$, has a $\xi^{\text{close}} \approx 0.58$. Since at the onset of buckling $\xi = 2/9$ [13], the transient regime of the kink, which is the focus of this work, is thus given by

$$\frac{2}{9} < \xi^{\text{kink}} < \xi^{\text{close}}, \quad (9)$$

or equivalently, by (7),

$$0 < \tilde{\kappa} < 1. \quad (10)$$

4. Kink's potential

The electronic band-structure of bent and buckled tubes was studied by many authors and analysed at depth recently by us (see [3] and citations therein).

To summarize it briefly, pure bending has no net strain but it does affect the bandgap as follows: bending causes ovalization of the cross-section – which increases the overall circumferential curvature – which is what affects the bandgaps; it was shown [3] that bandgaps, initially $\propto \cos 3\alpha/R^2$, become $\propto (1 + \frac{9}{2}\xi^2) \cos 3\alpha/R^2$, where ξ is the ovalization parameter (fig. 1d). In the pre-buckling regime, $\xi \propto \kappa^2$ so that the change due to bending is $\propto \kappa^4$. At post-buckling, however, the bulk (not including the kink) is independent of further bending and remains at the critical ovalization, $\xi = 2/9$; while the at kink $\xi^{\text{kink}} - 2/9 \propto \tilde{\kappa}^{1/2}$ (eq. 6). Hence, not too far from criticality, the bandgap at the kink changes as $\propto (\xi^{\text{kink}} - 2/9)^2 \propto \tilde{\kappa}^{1/2} \cos 3\alpha/R^2$.

With the above in mind, we apply next the general analysis in [3] to the zigzag (10,0). Its bandgap, Fermi energy and ovalization as a function of bending curvature are given in fig. (3). For tubes of this size ($R = 4\text{\AA}$) and smaller, Fermi energy downshifts in tandem with the bandgap as $\Delta E_F = \Delta E_g/2$, which is $\propto \kappa^4$ at the pre-buckling stage; its physical origin is the increased $\sigma - \pi$ hybridization at large circumferential curvatures, which at sufficiently large bending vanishes the bandgap entirely and downshifts the Fermi energy.

Fig. (3) also reveals the evolution of the ovalization parameter ξ ; at pre-buckling, $\xi \propto \kappa^2$ up to the onset of buckling – where $\xi = 2/9$ [13]; at post-buckling, away from the kink ξ remains constant while at the kink, $\xi^{\text{kink}} \propto \tilde{\kappa}^{1/2}$, where $\tilde{\kappa}$ is the post-buckling dimensionless bending (eq. 10). One can also observe that the bandgap at the kink vanishes when the its ovalization is $\xi^{\text{kink}} \gtrsim 4/9$. That will

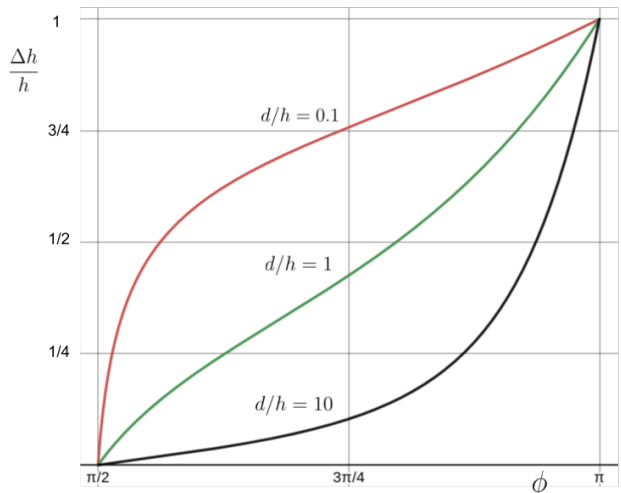


Figure 2: Change of height vs. wetting angle ϕ for a number initial aspect ratios.

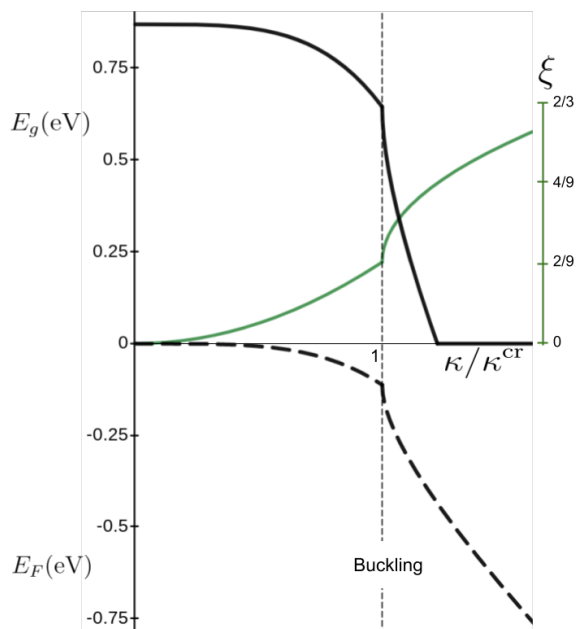


Figure 3: The bandgap E_g (full line), Fermi energy E_F (broken line) and ovalization parameter ξ (green) of a (10,0) tube under bending κ . The post-buckling section ($\kappa/\kappa^{\text{cr}} > 1$) corresponds to the kink.

For the (10,0) tube (and other tubes of similar radius), Fermi energy was found to downshift due to bending-induced ovalization by

$$E_F(\xi) = \frac{9C_s\xi^2}{4R^2} \cos 3\alpha, \quad (11)$$

where $C_s = 8 (\text{\AA}^2 \cdot \text{eV})$, α is the chiral angle and ξ is the ovalization parameter (fig. 1d). In buckled tubes the

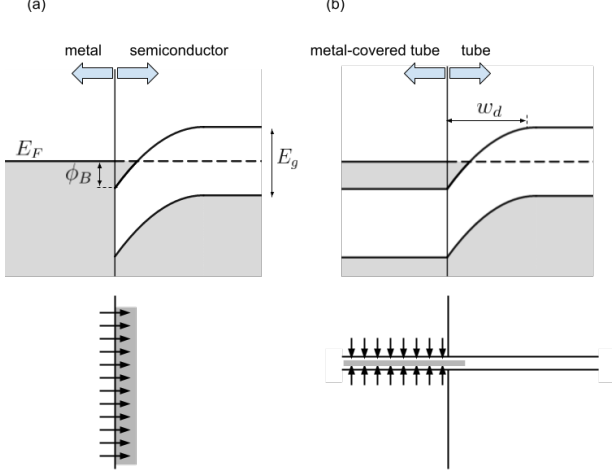


Figure 4: Comparing conventional metal-semiconductor interface (a) with a one with semiconducting CNT (b). Lower panels show the respective orientation of the interface dipoles.

kink is highly ovalized results in a difference in Fermi energy with the bulk,

$$\Delta E_F = \frac{9C_s}{4R^2} \left(\left(\frac{2}{9} \right)^2 - (\xi^{\text{kink}})^2 \right) \cos 3\alpha, \quad (12)$$

where the ovalization parameter at the bulk is, at the post-buckling stage, is fixed roughly at its value at the onset of buckling $\xi = 2/9$ [13].

The potential difference between the kink and the bulk is thus,

$$V_\kappa = -\Delta E_F + \frac{1}{2}\Delta E_g = -2\Delta E_F, \quad (13)$$

Substituting eq. (6) in (12), eq. (13) becomes

$$\begin{aligned} V_\kappa &= -\frac{2C_s}{R^2} \left(\xi^{\text{close}} - \frac{2}{9} \right) \tilde{\kappa}^{1/2} \cos 3\alpha, \\ &\approx -\frac{2C_s \tilde{\kappa}^{1/2}}{3R^2} \cos 3\alpha, \end{aligned} \quad (14)$$

where in the second row we substituted ξ^{close} for its value for the (10,0) tube (see text after eq. 8).

5. Bound state

The width W of the kink potential V_κ (eq. 14) is of the order of the tube diameter $\sim 1\text{nm}$. If the Fermi wavelength is much larger, the potential can be approximated

to a δ -function. Indeed, a class of tubes have their k_F zone-folded to zero: tubes that satisfy [15]

$$\text{gcd}(2m+n, 2n+m) = \text{gcd}(n, m), \quad (15)$$

where gcd is the greatest common divisor. All zigzag tubes ($m=0$), for example, meet this condition. Hence, for these tubes, the actual wavelength of the tunneling electrons is the thermal length, $\lambda_{\text{th}} = \sqrt{2\pi\hbar^2/m^*kT}$, where m^* is the effective mass at the band-edge: $m^* = \hbar^2(\partial^2 E/\partial k^2)^{-1} = 2\hbar^2\Delta k_y/(a\gamma\sqrt{3})$, where the energy spectrum of the π band, $E = \frac{\sqrt{3}}{2}a\gamma\sqrt{\Delta k_y^2 + k^2}$ was used (for simplicity, the effective mass is assumed not to change significantly by mixing with the singlet band); now since $\Delta k_y = E_g/(a\gamma\sqrt{3})$, one gets,

$$m^* = \frac{2\hbar^2 E_g}{3a^2\gamma^2}, \quad (16)$$

which gives, for $E_g = 1\text{eV}$, $m^* = 0.09m_e$, where m_e is the electron mass; the thermal length is then

$$\lambda_{\text{th}} = \sqrt{\frac{3\pi a^2 \gamma^2}{E_g kT}}, \quad (17)$$

giving $\lambda_{\text{th}} \approx 29\text{ nm}$ at liquid-nitrogen temperatures while $\lambda_{\text{th}} \approx 15\text{ nm}$ at room-temperature. Hence, even at room temperature $\lambda_{\text{th}} \gg W$, thus justifying its δ -function approximation.

Thus, considering the kink potential well as a δ -function with height V_κ (eq. 14) and width $W = 2R$, the wavefunction of the bound-state is then given by

$$\begin{aligned} \psi &= \sqrt{\frac{c}{2\pi R}} \exp(-c|z|), \quad \text{where} \\ c &= \frac{4E_g V_\kappa R}{3a^2\gamma^2}. \end{aligned} \quad (18)$$

A (10,0) tube, for example, having $E_g \approx 1\text{eV}$, $V_\kappa = 2\Delta E_F \approx 1\text{eV}$ (see fig. 3) and $R = 4\text{\AA}$, gives $c \approx 1\text{nm}^{-1}$.

The δ -function potential of area $V_\kappa W$ has at least one bound state of energy

$$E_\kappa = -\frac{m^* V_\kappa^2 W^2}{2\hbar^2} = -\frac{4E_g V_\kappa^2 R^2}{3a^2\gamma^2} \quad (19)$$

where the effective mass was substituted by eq. 16. For the same (10,0) tube and bending as in the example after eq. (18), this gives $E_\kappa = -0.38\text{eV}$.

6. Single ion perturbation

How is an ion passing through the open kink will affect the current? The surface potential due to an ion of charge $-1e$ at the center of the kink is

$$\Phi = \frac{k_e e^2}{\epsilon_r \sqrt{R^2 + z^2}} \quad (20)$$

where $k_e = 8.987 \times 10^9 \text{N}\cdot\text{m}/\text{C}^2$, and ϵ_r is the relative dielectric permittivity. It perturbs the bound state by

$$\begin{aligned} \Delta E_\kappa &= \int \psi^2 \Phi dz \\ &= 2\pi RW \psi^2(0) \Phi(0) = \frac{8k_e \epsilon^2 E_g V_\kappa R}{3\epsilon_r a^2 \gamma^2} \end{aligned} \quad (21)$$

where in the second row Φ was taken as a local potential (as we did with V_κ) extending throughout a ring of width W at the center of the kink. Returning to the (10,0) tube and applying eq. (21), we get $\Delta E_\kappa \sim 0.27 \text{eV}$ for a typical value of $\epsilon_r \approx 10$. This is a large perturbation as it is comparable with the zero-order energy level $E_\kappa = 0.38 \text{eV}$ (after eq. 19).

7. Contacts

The electronic transport depends, to a large extent, on the metal-nanotube contact. Experiments with such contacts demonstrated the differences with conventional metal-semiconductor interface but also resulted often in contradictory conclusions [16]. Some of this could be attributed to the fact that while tube diameter was usually known, its chiral angle was not (semiconducting tubes of equal diameter but different chirality give different work-functions [3]).

Nevertheless, the nature of the metal-CNT contact can be outlined and compared with the much-studied bulk metal-semiconductor interface (fig. 4a). Here, different work-functions across the interface result in Schottky barriers [17]

$$\phi_{B,n} = \phi_m - \chi - eD_{\text{int}} \quad (22)$$

$$\phi_{B,p} = E_g - \phi_{B,n} \quad (23)$$

where $\phi_{B,n}$ or $\phi_{B,p}$ are the Schottky barriers for n or p type semiconductors, χ is the semiconductor's electron affinity, ϕ_m the metal work-function and D_{int} is the density of electrostatic dipoles at the interface – a consequence of metallic Bloch surface states that decay into the semiconductor (in the so-called electron-accumulation region).

Consider now the metal-CNT contacts, where the CNT is covered by a metal electrode (fig. 4b). It was studied, for example, by measuring the Schottky barriers at contacts between the same CNT and electrodes of different materials – Hf, Cr, Ti and Pd [18]. It was found that electrodes with low work-function such as Hf (where metal-CNT dipoles should be largest), induce a conducting region within the metal-covered nanotube, akin to the electron-accumulation region in bulk interfaces. This seem to extend within the metal-covered region of the tube up to about 100nm [19]. Next to it, in the uncovered segment of the nanotube, lies the ideal Schottky barrier, extended throughout the depletion length (w_d in fig. 4b).

Thus, the resulting electron transport at the metal-CNT interface consists of crossing two barriers in series:

first, tunneling between the metal and the conduction region within the metal-covered tube (which takes place anywhere within a distance of $\sim 100\text{nm}$ from the free tube), and second, tunneling between this region and the free tube across the Schottky barrier.

8. Depletion region

Let us now estimate the depletion region in the free tube near an electrode. Say the electrode covers the tube at $z \leq 0$, then Poisson equation gives

$$-\frac{d^2\phi}{dz^2} = \frac{\rho(z)}{\epsilon} \quad (24)$$

and the charge density ρ is assumed constant in each of the two segments,

$$\rho(z) = \begin{cases} -eN_m, & z \leq 0 \\ eN_f, & 0 < z < w_d \end{cases}$$

where N_m and N_f are the charge densities in the segment covered by metal and free, respectively, and w_d is the depletion region. Solving for ϕ one gets,

$$w_d = \left(\frac{2\epsilon\phi_B}{e \left(N_f + \frac{N_f^2}{N_m} \right)} \right)^{1/2} \quad (25)$$

Assuming the tube is not doped, with $E_g \sim 1\text{eV}$, N_f is given by

$$N_f = \int_{E_c}^{\infty} g(E) e^{-(E-E_c)/kT} dE \quad (26)$$

where $g(E)$ is the density of states and E_c is the conduction band energy above the chemical potential. Now since $E_c - E_F \gg kT$ (in 10,0 tube, $E_c - E_F \sim 0.45\text{eV} \gg kT$ even at room temperature), $w_d \gtrsim 10^{-7}\text{m}$. This region is much larger than the length where tunneling can be effective. Thus, the tunnel junctions length l is assumed here to be $l \ll w_d$.

9. A short asymmetric junction

Fig. 5 depicts an asymmetric short junction ($l \ll w_d$), where the source and drain consists of metals with low and high work-functions, respectively (see appendix for work-functions).

Ignoring for the moment the kink and its bound state, charge transport in this junction (fig. 5) consists of the following. First, tunneling from the metal electrode at the source into the metal-induced n -states in the nanotube (of depth $\phi_{B,p}$), then tunneling through the free section of the tube into the metal-induced p -states in the tube, and finally tunneling out to the metal electrode at the drain.

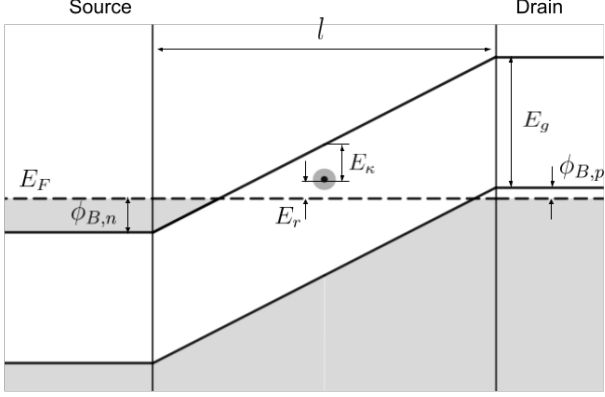


Figure 5: A semiconducting tube in an asymmetric junction: the source is a low work-function metal, such as Hafnium, and the drain is metal with a small barrier, such as Pd. The depicted junction is short ($l \ll w_d$).

Now adding the kink – with its bound state at depth E_κ below the conduction band – and a bias V between source and drain (fig. 6), we get the following conduction regimes. The height of the kink state above the Fermi energy at the source is

$$E_r = \frac{1}{2}(E_g + \phi_{B,p} - \phi_{B,n} - V) - E_\kappa \quad (27)$$

while relative to the conduction edge it is $E_r + \phi_{B,n}$. This sets the range of the "On" state, $-\phi_{B,n} \leq E_r \leq 0$, that is

$$-\phi_{B,n} \leq 2E_\kappa - E_g - \phi_{B,p} + V \leq \phi_{B,n} \quad (28)$$

When, at a larger bias, the junction is out of the "On" range, the bound state in the kink lies under the conduction band edge (fig. 6b), and the current decays exponentially.

A point of special interest is where the negative differential resistance is maximum. This occurs where E_r crosses the band edge of the source, which is just beyond the right-hand inequality of the resonance condition (28),

$$2E_\kappa \gtrsim E_g + \phi_{B,p} + \phi_{B,n} - V. \quad (29)$$

Eq. (29) gives the bias region at which the junction's negative differential resistance peaks. Hence, at this point the current's response to the ionic perturbation of the bound state is highest.

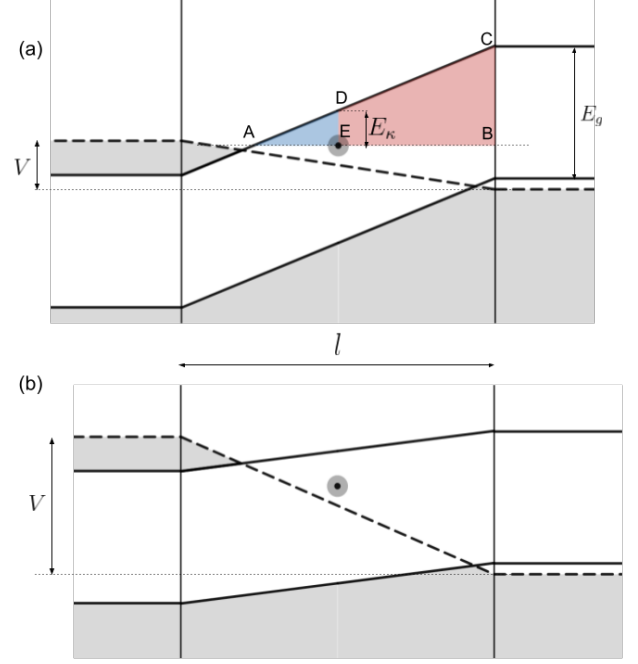


Figure 6: Band structure vs. drain-source bias at resonance (a) and valley (b). The resonance condition is given by eq. (28). The blue and red areas are tunneling barriers with transmissions given by eqs. (31) and (32), respectively.

10. Current and ionic perturbation

In our asymmetric junction, the direct tunneling between source and drain, ignoring the kink, would be under the triangle ABC (fig. 6a). The energy BC is $E_g - E_r$ (eq. 27) which is, within the WKB approximation and at zero bias,

$$\begin{aligned} T_{sd} &\approx \exp\left(-2 \int_A^B |k(z)| dz\right) \\ &= \exp\left(-\frac{4\sqrt{2}l}{3\hbar} \sqrt{m^*(E_g - E_r)}\right) \\ &= \exp\left(-\frac{4l(E_g + 2E_\kappa - \phi_{B,p} + \phi_{B,n} + V)}{3\sqrt{3}a\gamma}\right) \\ &\approx \exp\left(-\frac{8l(E_g + \phi_{B,n})}{3\sqrt{3}a\gamma}\right), \end{aligned} \quad (30)$$

where the last step assumes near resonance (eq. 29).

Within the "On" range (eq. 28), the tunneling between source and kink (at the center of the junction: fig. 6a) is

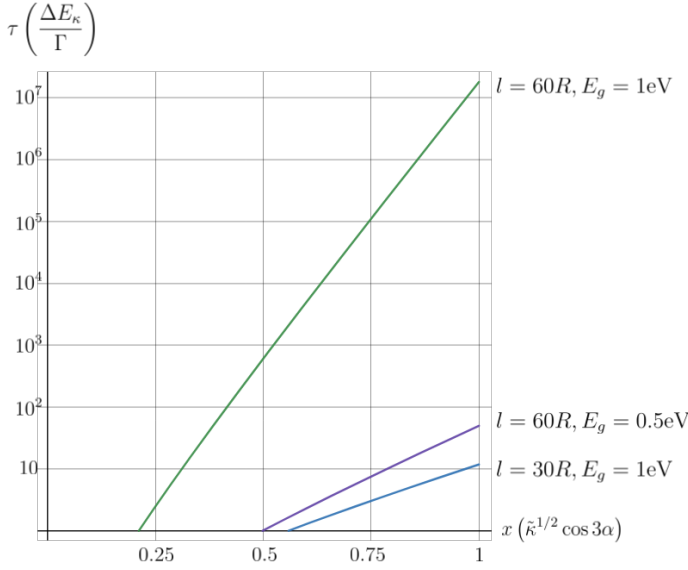


Figure 7: τ is a dimensionless shift of the bound level due to a single ion inside the kink, plotted here vs. post-buckling curvature $x \equiv \tilde{\kappa}^{1/2} \cos 3\alpha$, for a number of junction lengths l and bandgaps.

under the triangular potential ADE, which is,

$$\begin{aligned}
 T_{s,k} &\approx \exp\left(-2 \int_A^E |k(z)| dz\right) \\
 &= \exp\left(-\frac{4l}{3\sqrt{2}\hbar} \sqrt{m^* E_\kappa}\right) \\
 &= \exp\left(-\frac{8lE_g C_s \sqrt{\tilde{\kappa}} \cos 3\alpha}{9Ra^2\gamma^2}\right) \quad (31)
 \end{aligned}$$

where in the last step we substituted eq. (16) for m^* and eq. (19) for E_κ .

The tunneling between kink and drain (red area in fig. 6a) is

$$\begin{aligned}
 T_{k,d} &\approx \exp\left(-2 \int_E^B |k(z)| dz\right), \\
 &= \exp\left(-2 \left(\int_A^B |k(z)| dz - \int_A^E |k(z)| dz\right)\right), \\
 &= \frac{T_{sd}}{T_{s,k}}, \\
 &= \exp\left(-\frac{8l}{3\sqrt{3}a\gamma} (E_g(1 - \epsilon_\kappa) + \phi_{B,n})\right), \quad (32)
 \end{aligned}$$

where

$$\epsilon_\kappa \equiv \frac{C_s \sqrt{\tilde{\kappa}} \cos 3\alpha}{\sqrt{3}a\gamma R} \ll 1. \quad (33)$$

For $R = 4\text{\AA}$, for example, $\epsilon_\kappa = 0.15\sqrt{\tilde{\kappa}} \cos 3\alpha$; but $\sqrt{\tilde{\kappa}} \cos 3\alpha \leq 1$ ($\tilde{\kappa} = 1$ corresponds to the kink's closure), hence $\epsilon_\kappa \ll 1$ holds everywhere.

The current per channel is given by

$$I = \frac{2e}{\hbar} \int T(E)[f_s(E) - f_d(E)]dE \quad (34)$$

where $f_s(E), f_d(E)$ are the Fermi distributions at the source/drain, respectively.

Near resonance, the total transmission probability per channel is given by [20],

$$T(E) = \frac{\Gamma_s \Gamma_d}{(E - E_r)^2 + \left(\frac{\Gamma_s + \Gamma_d + \Gamma_\phi}{2}\right)^2} \quad (35)$$

where E_r is given by eq. 27, and Γ_s, Γ_d are the coupling of the kink state to the source/drain, respectively, and Γ_ϕ is the electron-phonon coupling. The source/drain coupling is given by

$$\begin{aligned}
 \Gamma_s &= \frac{\hbar v_F}{W} T_{s,k} \\
 \Gamma_d &= \frac{\hbar v_F}{W} T_{k,d} \quad (36)
 \end{aligned}$$

where v_F is the Fermi velocity and W is the width of the kink potential well ($\sim 2R$). With $v_F = 10^6\text{m/s}$, $R = 4\text{\AA}$ (for a (10,0) tube), $l = 20\text{nm}$, $E_g = 0.8\text{eV}$ and $E_\kappa = 0.4\text{eV}$, eqs. (36) give $\Gamma_s = 7.5 \cdot 10^{-6}\text{eV}$ and $\Gamma_d = 5 \cdot 10^{-10}\text{eV}$.

The overall current depends sensitively, in addition to the factors treated here, also on the electron-phonon coupling. The peak current, however, is independent of this coupling [20], and is given by,

$$I_p = \frac{2e}{\hbar} \frac{\Gamma_s \Gamma_d}{\Gamma_s + \Gamma_d} \approx \frac{e v_F T_{k,d}}{R}, \quad (37)$$

where Γ_s, Γ_d are given by eq. (36), and in the approximation, $\Gamma_s \gg \Gamma_d$ was assumed, as in eq. (39).

11. Figure of merit

A simple measure of sensitivity to the presence of an ion is the quantity

$$\tau \equiv \frac{\Delta E_\kappa}{\Gamma} \quad (38)$$

τ gives the shift in the bound state energy due to an ion in the center of the kink, divided by its width $\Gamma = \Gamma_s + \Gamma_d$ (eq. 36). Substituting ΔE_κ from eq. (21), $T_{s,k}$ (31) in Γ_s , and since $\Gamma_s \gg \Gamma_d$, $\Gamma \approx \Gamma_s$, hence,

$$\tau = \frac{16k_e e^2 E_g V_\kappa R^2}{3\epsilon_r a^2 \gamma^2 \hbar v_F} \exp\left(\frac{8lE_g V_\kappa R}{9a^2 \gamma^2}\right), \quad (39)$$

or,

$$\tau = (a_e a_g x) \exp\left(\frac{8la_g x}{9R}\right), \quad \text{where,} \quad (40)$$

$$x \equiv \tilde{\kappa}^{1/2} \cos 3\alpha,$$

$$a_e \equiv \frac{16k_e e^2}{3\epsilon_r \hbar v_F} \approx 1.16,$$

$$a_g \equiv \frac{C_s E_g}{a^2 \gamma^2},$$

where, if $E_g = 1\text{eV}$, for example, $a_g = 0.14$. τ is depicted in fig. (7) for a number of junction lengths and bandgaps as a function of post-buckling bending. Clearly, τ is largest for long junctions and high bandgaps. However, being a tunneling junction, this also translates to an exponentially weaker signal (eq. 37). Thus, τ and I_p are the two quantities that need to be traded-off.

12. Conclusion

We proposed here a solid-state nanopore device based on buckled semiconducting CNT, and a method of fabricating it at scale. An open kink is an ovalized constriction – in-effect, a nanopore within a nanotube; in addition, open kinks in semiconducting tubes have a localized bound state within the bandgap. Ions translocat-

ing the kink will electrostatically perturb this state. The response of the current to this perturbation is the signal; it can be maximized under certain conditions explored here, in particular, biasing an asymmetric tunnel junction to the negative differential resistance regime, near the resonance point.

Compared with existing solid-state nanopore devices, this has two principle novelties: first, it provides a nanoscale constriction (effectively a nanopore within a nanotube) whose cross-section is smooth and adjustable. And second, the modulated current is not ionic but electronic.

Appendix A: Schottky barriers for zigzag tube

This appendix includes data concerning the *ideal* contacts between a range of semiconducting zigzag tubes and a number of selected metals. It is listed in table I and depicted for a few selected metals in fig. (8).

The variation in Schottky barrier height among the tubes is due to two factors: bandgap and Fermi level. Now bandgap, which is $\propto 1/R$ for large n , increased the electron affinity χ , by the same measure. For small n , in contrast, bandgaps are lower but so is the Fermi level ([3] and references therein). Hence the lowering of the Schottky barrier height.

-
- [1] Y.-L. Ying, Z.-L. Hu, S. Zhang, Y. Qing, A. Fragasso, G. Maglia, A. Meller, H. Bayley, C. Dekker, and Y.-T. Long, Nanopore-based technologies beyond dna sequencing, *Nature Nanotechnology* **17**, 1136 (2022).
- [2] A. Fragasso, S. Schmid, and C. Dekker, Comparing current noise in biological and solid-state nanopores, *ACS Nano* **2020** **14**, 1338–1349 (2020).
- [3] A. Kleiner, Bandgaps of bent and buckled carbon nanotubes, arXiv:2301.05085 [cond-mat.mes-hall] (2023).
- [4] A. Kleiner, Transistor and nanopore based on kinks in nanotubes and method of making the same, European Patent Office, International application no. PCT/EP2021/025469 (2021).
- [5] B. I. Yakobson, C. J. Brabec, and J. Bernholc, Nanomechanics of carbon tubes: Instabilities beyond linear response, *Phys. Rev. Lett.* **76** (1996).
- [6] Z. Tu, O. Chun, and Z. C. Yang, Single walled and multiwalled carbon nanotubes viewed as elastic tubes with the effective Young’s moduli dependent on layer number, *Phys. Rev. B* **65**, 233407 (2002).
- [7] C. Guoxin and C. Xi, Buckling of single-walled carbon nanotubes upon bending: Molecular dynamics simulations and finite element method., *Phys. Rev. B* **73**, 155435 (2006).
- [8] Y. Zhang, C. M. Wang, W. H. Duan, Y. Xiang, and Z. Zong, Assessment of continuum mechanics models in predicting buckling strains of single-walled carbon nanotubes, *Nanotechnology* **20** (2009).
- [9] S. Iijima, C. Brabec, A. Maiti, and J. Bernholc, Structural flexibility of carbon nanotubes., *The Journal of Chemical Physics* **104**, 2089 (1996).
- [10] M. M. J. Treacy, T. W. Ebbesen, and J. M. Gibson, Exceptionally high Young’s modulus observed for individual carbon nanotubes., *Science* **381**, 678 (1996).
- [11] S. Zhang, R. Khare, T. Belytschko, J. Hsia K., S. L. Mielke, and G. C. Schatz, Transition states and minimum energy pathways for the collapse of carbon nanotubes, *Phys. Rev. B* **73**, 075423 (2006).
- [12] C. R. Calladine, *Theory of shell structures* (Cambridge University Press, 1989).
- [13] L. G. Brazier, On flexure of thin cylindrical shells and other thin sections, *Proceedings of the royal society of London, series A* **116**, 104 (1927).
- [14] A. Kutana and K. P. Giapis, Transient deformation regime in bending of single-walled carbon nanotubes., *Phys. Rev. Lett.* **97** (2006).
- [15] R. A. J. et. al., Electronic and lattice properties of carbon nanotubes, *J. Phys. Soc. Jpn.* **63**, 2252 (1994).
- [16] J. Svensson and E. E. B. Campbell, Schottky barriers in carbon nanotube-metal contacts, *J. Appl. Phys.* **110**, 111101 (2011).
- [17] S. M. Sze and K. K. Ng, *Physics of semiconductor devices*, John Wiley and Sons (2007).
- [18] D. J. P. et al., Anomalous schottky barriers and contact band-to-band tunneling in carbon nanotube transistors, *ACS Nano* **4**, 3103 (2010).
- [19] A. D. Franklin and Z. Chen, Length scaling of carbon nanotube transistors, *Nat. nano.* **5**, 858 (2010).

n	7	8	10	11	13	14	16	17	19	20
E_g	0.474	0.853	0.913	0.945	0.714	0.733	0.586	0.6	0.497	0.5
χ	4.803	4.373	4.243	4.187	4.303	4.293	4.367	4.36	4.411	4.407
ϕ_m	$\phi_B = \phi_m - \chi$									
Pt 5.65	0.847	1.276	1.406	1.462	1.347	1.356	1.283	1.29	1.238	1.243
Pd 5.12	0.317	0.747	0.876	0.932	0.817	0.827	0.753	0.76	0.709	0.713
Au 5.1	0.297	0.726	0.856	0.912	0.797	0.806	0.733	0.74	0.688	0.693
Ag 4.26	-0.543	-0.113	0.016	0.072	-0.043	-0.0335	-0.107	-0.1	-0.151	-0.147
Ga 4.2	-0.603	-0.173	-0.043	0.013	-0.013	-0.093	-0.167	-0.16	-0.211	-0.207
Mg 3.66	-1.143	-0.713	-0.583	-0.527	-0.643	-0.633	-0.707	-0.7	-0.751	-0.747
Li 2.9	-1.903	-1.473	-1.343	-1.287	-1.403	1.393	1.467	-1.46	-1.511	-1.507
K 2.3	-2.503	-2.073	-1.943	-1.887	-2.003	-1.993	-2.067	-2.06	-2.111	-2.107

Table I: A list of ideal Schottky barriers between various metals and zigzag tubes $(n, 0)$. Energy gaps and electron affinity χ are calculated according to [3] while work function (ϕ_m) are taken from [21].

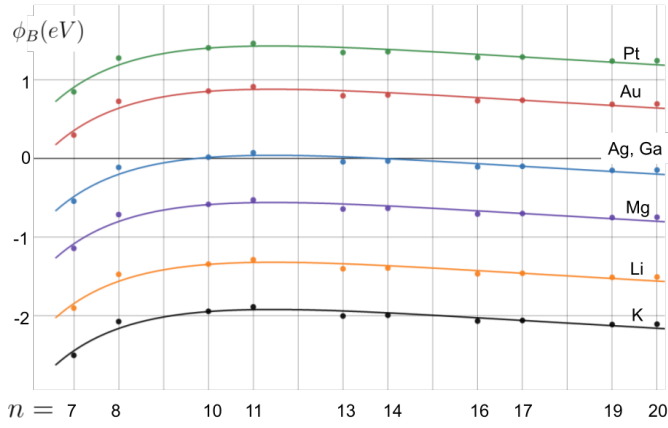


Figure 8: Ideal Schottky barrier heights ϕ_B between semiconducting zigzag tubes and various metals (according to the data in table I). Every number n represents a $(n, 0)$ semiconducting tube.

[20] S. Datta, *Electronic transport in mesoscopic systems*, Cambridge University Press (2001).

[21] H. B. Michaelson, Relation between an atomic electronegativity scale and the work function, *IBM J. Res. Dev.* **22**, 72 (1978).